

Experimental characterization of quantum dynamics through many-body interactions

Daniel Nigg¹, Julio T. Barreiro^{1,*}, Philipp Schindler¹, Masoud Mohseni^{3,†}

Thomas Monz¹, Michael Chwalla^{1,2}, Markus Hennrich¹, and Rainer Blatt^{1,2}

¹*Institut für Experimentalphysik, Universität Innsbruck, Technikerstrasse 25, A-6020 Innsbruck, Austria*

²*Institut für Quantenoptik und Quanteninformation der Österreichischen Akademie der Wissenschaften, Technikerstrasse 21a, A-6020 Innsbruck, Austria*

³*Research Laboratory of Electronics, Massachusetts Institute of Technology, Massachusetts 02139, USA*

(Dated: Wednesday 16th June, 2021)

We report on the implementation of a quantum process tomography (QPT) technique known as direct characterization of quantum dynamics (DCQD) applied on coherent and incoherent single-qubit processes in a system of trapped $^{40}\text{Ca}^+$ ions. Using quantum correlations with an ancilla qubit, DCQD reduces exponentially the number of experimental configurations required for standard QPT. With this technique, the system's relaxation times T_1 and T_2 were measured with a single experimental configuration. We further show the first complete characterization of single-qubit processes using a single generalized measurement realized through multi-body correlations with three ancilla qubits.

PACS numbers: 03.67.Ac; 03.65.Wj

Characterization of quantum dynamics is an important primitive in quantum physics, chemistry, and quantum information science for determining unknown environmental interactions, estimating Hamiltonian parameters, and verifying the performance of engineered quantum devices. This has led to a major effort in developing tools for the full characterization of quantum processes, known as quantum process tomography (QPT). The standard approach for QPT is resource intensive, requiring 12^N experimental configurations for a system of N qubits [1, 2], where each experimental configuration consists of the preparation of input probe states and the measurement of process outputs. Using ancilla qubits but only joint separable measurements, the number of experimental configurations is still 12^N [3–5]. However, the use of many-body interactions to ancilla qubits in the preparation and/or measurements can significantly decrease this number to anywhere from 4^N to a single configuration depending on the nature and complexity of quantum correlations [5]. Using two-body correlations DCQD requires up to 4^N experimental configurations for full quantum process tomography, and in particular only one experimental setting for estimating certain parameters (e.g. relaxation times) [6, 7] (see Ref. [8, 9] for partial and non-scalable implementations of DCQD).

Alternative tomographic methods such as randomized benchmarking [10], selective and efficient QPT [11, 12] and compressed sensing for quantum process tomography [13–15] have recently been developed to overcome the exponential increase of the required experimental configurations. Generally, these methods are tailored to estimate a polynomial number of effective parameters, such as gate fidelity [10] or when we can make a sparse quantum process/Hamiltonian assumption from a priori knowledge about the quantum system [15]. For example, the estimation of the dynamical parameters T_1 and

T_2 (longitudinal and transverse relaxation times [1]) is a task involving two non-commuting observables (e.g. σ_x and σ_z) that cannot be measured simultaneously. These parameters describe the influence of noise on atomic-, molecular- and spin-based systems induced by the interaction with the environment. An alternative approach based on DCQD, henceforth called Direct Characterization of Relaxation Times (DCRT), enables the measurement of both T_1 and T_2 *simultaneously* with a single experimental configuration [16].

In this work, we apply the DCQD technique and extensions on a system of trapped $^{40}\text{Ca}^+$ ions. Single-qubit processes are reconstructed with four experimental configurations using DCQD, and alternatively with just a single configuration using a generalized measurement (GM). In addition, we quantify the relaxation times T_1 and T_2 in our system with a single configuration. This technique can also characterize more realistic environments affecting not only the probe but also the ancilla qubit collectively.

Every process acting on a quantum system can be described by a complete positive map E mapping the input state ρ onto the output state ρ' . For a single qubit this can be written as

$$E : \rho \rightarrow \rho' = \sum_{m,n=1}^4 \chi_{m,n} \sigma_m \rho \sigma_n^\dagger, \quad (1)$$

with σ_m , σ_n the Pauli operators $\{\mathbb{1}, \sigma_x, \sigma_y, \sigma_z\}$ and χ a semi-positive matrix containing complete information about the process. In standard quantum process tomography (SQPT) the process is applied to four input states and followed by full state tomography of each output state, which for a trace preserving map consists of three measurements, resulting in $4 \times 3 = 12$ experimental configurations. In DCQD these four input states are replaced

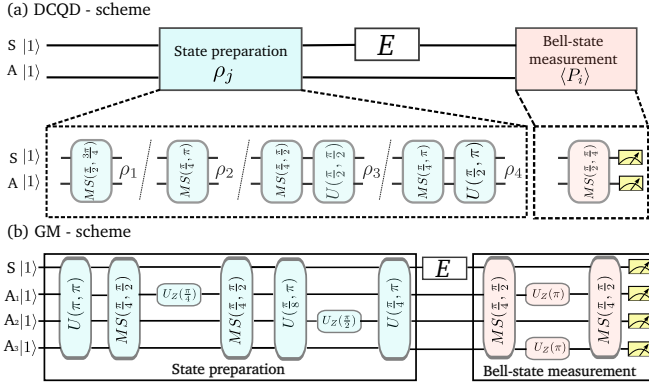


FIG. 1. (color online) Procedure to characterize a single-qubit process with DCQD and a GM. In DCQD (a) each experimental configuration consists of the preparation of one of four input states ρ_j entangled between the system ion S and the ancilla ion A. The process E is applied on S followed by a BSM on the output state $E(\rho_j)$, which consists of a single MS operation followed by a projection onto the computational basis. (b) Generalized measurement via many body interactions (see text).

by four entangled states between the system qubit S and an ancilla qubit A, and the state tomography is replaced by a single Bell-state measurement (BSM), as shown in Fig. 1(a), with a total of $4 \times 1 = 4$ experimental configurations (Bell states $|\Psi^\pm\rangle$ and $|\Phi^\pm\rangle$ as defined in Table I). The probabilities $p_{i,j}$ of measuring the Bell-state projector P_i for each input state ρ_j shown in Table I are determined, according to Refs. [6, 17], by

$$p_{i,j} = \text{Tr}(P_i E(\rho_j)) = \sum_{m,n=1}^4 \chi_{m,n} \Lambda_{m,n}^{i,j} \quad (2)$$

$$\Lambda_{m,n}^{i,j} = \text{Tr}(P_i(\sigma_m \otimes \mathbb{1})\rho_j(\sigma_n \otimes \mathbb{1})^\dagger).$$

Therefore the process matrix χ can be calculated directly by linear inversion of the matrix Λ . The set of input states ρ_j and the Bell-state projectors P_i have to be determined such that the 16 equations in Eq. (2) are linearly independent, which ensures that Λ is invertible (Table I).

Our experiments were realized on a system consisting of $^{40}\text{Ca}^+$ ions confined to a string in a linear Paul trap [18]. Each ion represents a logical qubit which is encoded in the electronic levels $D_{5/2}(m = -1/2) = |0\rangle$ and $S_{1/2}(m = -1/2) = |1\rangle$. Each experimental cycle consists of an initialization of the ions in their internal electronic and motional ground states followed by a coherent manipulation of the qubits and finally a detection of the quantum state. State initialization is realized by optical pumping into the $S_{1/2}(m = -1/2)$ state after cooling the axial centre-of-mass mode to the motional ground state. The manipulation of the qubits is implemented by coherently exciting the $S_{1/2} \leftrightarrow D_{5/2}$ quadrupole transition with laser pulses. Finally, the population of the qubit states is measured by exciting the $S_{1/2} \leftrightarrow P_{1/2}$ transi-

Input states $\rho_j = \psi_j\rangle\langle\psi_j $	Bell-state basis
$ \psi_1\rangle = 00\rangle + 11\rangle$	$ \Phi^+\rangle = 00\rangle + 11\rangle$
$ \psi_2\rangle = \alpha 00\rangle + \beta 11\rangle$	$ \Psi^+\rangle = 01\rangle + i 10\rangle$
$ \psi_3\rangle = \alpha ++\rangle_x - \beta --\rangle_x$	$ \Psi^-\rangle = 01\rangle - i 10\rangle$
$ \psi_4\rangle = \alpha ++\rangle_y - \beta --\rangle_y$	$ \Phi^-\rangle = 00\rangle - 11\rangle$

TABLE I. Input states and BSM basis used for the implementation of DCQD ($|\pm\rangle_x = \frac{|0\rangle \pm |1\rangle}{\sqrt{2}}$, $|\pm\rangle_y = \frac{|0\rangle \pm i|1\rangle}{\sqrt{2}}$). The determinant of Λ in Eq. (2) is maximized for $\alpha = \cos(\frac{3\pi}{8})$ and $\beta = \exp(i\frac{\pi}{2})\sin(\frac{3\pi}{8})$ to ensure the invertibility [17]. The BSM is realized by a measurement with the projectors $P_i = \{|\Phi^\pm\rangle\langle\Phi^\pm|, |\Psi^\pm\rangle\langle\Psi^\pm|\}$.

tion and detecting the fluorescence light, using electron shelving [19]. Our setup is capable of realizing collective qubit rotations $U(\theta, \phi) = \exp(-i\frac{\theta}{2} \sum_i [\sin(\phi)\sigma_y^{(i)} + \cos(\phi)\sigma_x^{(i)}])$ via a laser beam addressing the entire register as well as Mølmer-Sørensen entangling gates $MS(\theta, \phi) = \exp(-i\frac{\theta}{4} [\sum_i \sin(\phi)\sigma_y^{(i)} + \cos(\phi)\sigma_x^{(i)}]^2)$ [20, 21]. Additionally we are able to perform single-qubit rotations on the i -th ion of the form $U_Z^{(i)}(\theta) = \exp(-i\frac{\theta}{2}\sigma_z^{(i)})$ by an off-resonant laser beam, which addresses individual ions. The input states for DCQD of Table I are prepared by applying collective entangling operations and qubit rotations as shown in Fig. 1(a). For example, the input state ρ_2 is created by the non-maximally entangling operation $MS(\frac{\pi}{4}, \pi)$. Our two-qubit entangling operation generates Bell states with a fidelity of $\approx 99\%$ in 120 μs .

The BSM is experimentally realized by a maximally entangling operation $MS(\frac{\pi}{2}, \frac{\pi}{4})$, which maps from the Bell-state basis to the computational basis $\{|00\rangle, |01\rangle, |10\rangle, |11\rangle\}$, followed by individual-ion-resolving fluorescence detection with a CCD camera. For example, consider the first input state $\rho_1 = |\Phi^+\rangle\langle\Phi^+|$. If the process E is the identity $\mathbb{1}$, the expectation value of the BSM-projector P_1 is 1 which is equivalent to detecting both ions in the state $|11\rangle$ after the BSM. If a bit flip occurs on the system ion, the output state is then mapped onto the state $|01\rangle$ by the BSM ($\langle P_2 \rangle = 1$). The considerations are similar for a phase-flip, or bit- and phase-flip processes. Therefore, the diagonal elements $\chi_{m,m}$ of the superoperator χ corresponding to $\mathbb{1}$, σ_x , σ_y , and σ_z are detected by a single input state in combination with one BSM.

We demonstrate the DCQD method by characterizing the full quantum process of implemented unitary rotations σ_x and σ_y as well as non-unitary processes such as amplitude- and phase-damping [22]. The χ matrices reconstructed from the measured probabilities, are shown in Fig. 2(a,b) for σ_x and σ_y rotations. A single-qubit process can also be visualized by transforming the pure states lying on a Bloch sphere. In this Bloch sphere representation, decohering processes map the unit Bloch sphere (shown as a transparent mesh) to an ellipsoid of

smaller volume [1]. Implemented amplitude- and phase-damping processes taking place with a 60% probability are shown in this representation in Fig. 2(d,f) [22]. For each input state the experiment was repeated up to 250 times for statistical averaging. All processes were reconstructed with a maximum likelihood algorithm to ensure trace preservation and positivity of the superoperator χ [23]. The fidelity F of a process describes the overlap between the measured χ_{meas} and the ideal superoperator χ_{id} . For each process we calculate the overlap between χ_{meas} and χ_{id} using the Uhlmann-Jozsa fidelity with the Jamiolkowski isomorphism [23, 24]. Table II shows the calculated fidelities for the implemented DCQD and for SQPT. The uncertainty in the fidelity was estimated by parametric bootstrapping based on projection noise in our measurement [25].

Target process	DCQD, F (%)	SQPT, F (%)
$\mathbb{1}$	97.5 ± 0.6	98.1 ± 1.3
σ_x	96.5 ± 1.0	98.1 ± 1.3
σ_y	96.6 ± 1.4	97.5 ± 1.4
amplitude damping	95.3 ± 1.9	95.2 ± 2.7
phase damping	97.4 ± 0.8	95.7 ± 0.8

TABLE II. Calculated process fidelities F between implemented and target processes as characterized with DCQD and SQPT. All processes were measured with a total of 1000 experimental cycles, which correspond to 1000/4 cycles per experimental configuration for DCQD and 1000/(4×3)~84 for SQPT. The SQPT of the phase damping process was measured with a total of 3000 experimental cycles.

Full QPT of a single-qubit process is also possible with a single experimental configuration by using additional ancillas and a generalized measurement (GM). Here, we expand the dimension of the Hilbert space $H_A \otimes H_S$, with the system Hilbert space H_S and the ancilla Hilbert space H_A , such that the dimension of the total Hilbert space is equal to the number of free parameters in the process matrix χ [5]. For a single-qubit process one has to determine all 16 superoperator elements $\chi_{m,n}$ which leads to an 8 dimensional ancilla Hilbert space. Therefore we used three ancilla qubits A_1, A_2 and A_3 to quantify a full process E acting on the system qubit S . This GM is realized by entangling the system and ancilla qubits using many-body interactions [20, 21], then applying the process E on S and finally performing BSMs on two pairs. Figure 1(b) shows the sequence implemented for this GM which proceeds as follows. First, we create an entangled input state using maximally and non-maximally entangling Mølmer-Sørensen interactions in combination with global and addressed single-qubit rotations. After applying the process E on S we perform a pairwise BSM on the combined output state by implementing two non-maximally entangling operations $MS(\frac{\pi}{4})$ and two addressed AC-Stark pulses $U_Z^{(1)}(\pi)$ and $U_Z^{(3)}(\pi)$, which separate the entangled sys-

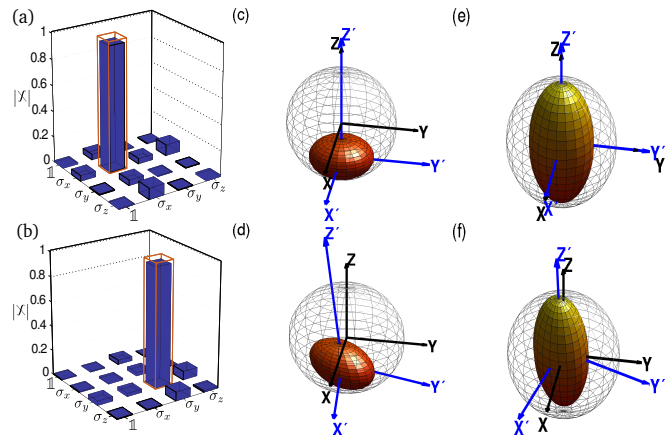


FIG. 2. (color online) Experimental results of DCQD for unitary and decoherence processes. (a-b) Results of the measured superoperator χ for the rotation operations $U(\pi, 0)$ in (a) and $U(\pi, \pi/2)$ in (b). Ideally, the target processes have only nonzero elements at positions indicated by the orange-bordered bars. (c-d) Bloch sphere representation of the ideal (c) and measured (d) amplitude damping process with 60% probability [22]. (e-f) Bloch sphere representation of the ideal (e) and measured (f) phase damping process with 60% probability [22]. Bloch sphere axes in black evolve into the spheroid primed axes in blue. A slight imperfection due to residual light on the ancilla ion can be observed as a rotation of the spheroids in the measured decohering processes.

tem $H(S, A_1, A_2, A_3)$ into a product state of two subsystems $H(A_1, A_3) \otimes H(S, A_2)$. These operations are equivalent to two pairwise maximally entangling gates $MS(\frac{\pi}{2})$ acting on the two subsystems $H(A_1, A_3)$ and $H(S, A_2)$. The 16 results of the measurement are directly linked to the 16 superoperator elements $\chi_{m,n}$ by a matrix Λ similar to Eq. (2). Using this technique we reconstructed unitary processes $\{\mathbb{1}, \sigma_x = U(\pi, 0), \sigma_y = U(\pi, \frac{\pi}{2}), \sigma_z = U_z^{(1)}(\pi)\}$ acting on a single qubit with a fidelity of $\{99.70 \pm 0.02, 97.30 \pm 0.29, 99.80 \pm 0.01, 99.40 \pm 0.02\}\%$. All processes were measured with a total of 5000 cycles.

In contrast to previous QPT measurements of engineered processes, the process of phase (amplitude) damping occurs naturally in our system due to magnetic field fluctuations (spontaneous decay) [26]. The dynamical parameters T_1 and T_2 can, however, be determined simultaneously with only the first input state ρ_1 being subject to the DCQD scheme even if the damping processes act collectively on both qubits (as in our experimental system [26]). This method, named DCRT above, consists of preparing an input Bell state $\rho_1 = |\Phi^+\rangle\langle\Phi^+|$, exposing both qubits to the damping processes for a time t and a final BSM, which yields the diagonal elements $\chi_{i,i}$ of the process matrix. As described in the supplementary material [22] and assuming Markovian noise the dynamical parameters are then given by

$$e^{-\frac{N^2 t}{T_2}} = \chi_{1,1} - \chi_{4,4} \quad (3)$$

$$= \text{Tr} \{ [|\Phi^+\rangle\langle\Phi^+| - |\Phi^-\rangle\langle\Phi^-|] E(|\Phi^+\rangle\langle\Phi^+|) \},$$

$$1 + 2e^{-\frac{2t}{T_1}} - 2e^{-\frac{t}{T_1}} = 1 - 2(\chi_{2,2} + \chi_{3,3}), \quad (4)$$

with N the number of ions. From the entries of the χ matrix corresponding to $\mathbb{1}$ and σ_z (σ_x and σ_y) operations, T_2 (T_1) depends on the probability that no error or phase flips (bit flips) occur on the entire system. A fit of DCRT measurements $\chi_{i,i}$ to Eqns. (3-4) at different times t thus yields T_1 and T_2 using a single experimental configuration. We explored this DCRT technique in our experimental system. The measurement results of the decoherence estimation are shown in Fig. 3(a). The green dots show the difference between the diagonal elements $\chi_{1,1}$ and $\chi_{4,4}$ as a function of the waiting time t . The spontaneous decay of the system is shown in Fig. 3(b) by plotting $1 - 2(\chi_{2,2} + \chi_{3,3})$ as a function of time. For every waiting time t the experiment was repeated up to 250 times to gain significant statistics.

We can compare the DCRT technique with two traditional methods that use product input states: Ramsey-contrast measurements for phase-decoherence estimation and direct spontaneous-decay measurements [27]. A Ramsey-contrast measurement is realized by initializing the ion in the state $(|0\rangle + |1\rangle)/\sqrt{2}$ by a global rotation $U(\frac{\pi}{2}, 0)$, followed by a waiting time t and finally applying a second rotation $U(\frac{\pi}{2}, \phi)$ in which the phase ϕ is varied. The observed contrast as a function of ϕ corresponds to the preserved phase coherence. Spontaneous-decay measurements, instead, consist of measuring the probability of detecting both ions in the excited state $|0\rangle$ as a function of time. The results of these Ramsey-contrast (spontaneous-decay) measurements are shown in Fig. 3(a) (Fig. 3(b)) as red diamonds (blue triangles). The measured relaxation times corresponding to the traditional methods are called T_1^{trad} and T_2^{trad} . The exponential fit (green line) of Eq. (3) to the data was estimated with $N = 2$ (collective dephasing) and yields $T_2^{\text{DCRT}} = 18.8(5)$ ms. The Ramsey-contrast measurements (red diamonds) were carried out on a single ion and yield a coherence time of $T_2^{\text{trad}} = 19.4(8)$ ms. The green dotted line in Fig. 3(a) corresponds to the fitted function to Eq. (3) (green line) with $N = 1$ instead of $N = 2$ and shows good agreement with the single-ion Ramsey-contrast measurement. Therefore the DCRT technique enables the characterization of the phase decoherence of the collective system (green line) and also gives a conclusion about the phase decoherence of a single ion (green dotted line). An exponential fit of the decay data of Fig. 3(b) to Eq. (4) gives the characteristic lifetime $T_1^{\text{DCRT}} = 1130(47)$ ms for the DCRT technique (green

line) and $T_1^{\text{trad}} = 1160(30)$ ms for the traditional method (blue dotted line), which are in good agreement with previously measured values [28] of 1148(18) ms.

In summary, we have experimentally demonstrated two different approaches for the full characterization of single-qubit quantum processes, lowering the required experimental configurations from 12 to 4 using DCQD and a single configuration via the GM method. The reconstruction of coherent and incoherent processes was shown with fidelities of $\geq 97\%$ using DCQD. In particular, we have observed a lower statistical uncertainty of the fidelity of some of the processes compared to the SQPT. Nevertheless, a matter of further investigations is a comparison of the scaling in the number of experimental cycles required for the SQPT and DCQD to achieve a target uncertainty in the fidelity (e.g. see identity process in Table II). The DCRT technique, based on the DCQD protocol, was used as a powerful tool to characterize the noise in our system by measuring the relaxation times T_1 and T_2 simultaneously with one experimental setting. This technique indicates good agreement with traditional methods as Ramsey-contrast and spontaneous decay measurement. In principle, there is an improvement of a factor of two in the measurement time if T_1 is of the same order of magnitude as T_2 , which is not the case for our setup. In contrast, spin-based solid state systems are collectively affected by noise and $T_1 \approx T_2$, which would lead to a significant improvement of the measurement time [29]. Another application of DCRT could be for biological systems where dissipative dynamics play a crucial role [30, 31]. The same measurement procedure can also be used as a tool to quantify Hamiltonian parameters efficiently [7, 16].

We gratefully acknowledge support by the Austrian Science Fund (FWF), through the Foundations and Applications of Quantum Science (SFB FoQus), by the European Commission AQUITE, by IARPA, QuISM MURI and DARPA QuBE Program as well as the Institut für Quantenoptik und Quanteninformation GmbH. Julio T. Barreiro acknowledges support by a Marie Curie International Incoming Fellowship within the 7th European Community Framework Programme.

* Current address: Quantum Optics Group, Ludwig-Maximilians-University; Julio.Barreiro@uibk.ac.at

† mohseni@mit.edu

- [1] M. A. Nielsen and I. L. Chuang, *Quantum Computation and Quantum Information* (Cambridge University Press, 2009)
- [2] A. M. Childs, I. L. Chuang, and D. W. Leung, Phys. Rev. A **64**, 012314 (2001)
- [3] G. M. D. Ariano and P. L. Presti, Phys. Rev. Lett. **86**, 4195 (2001)

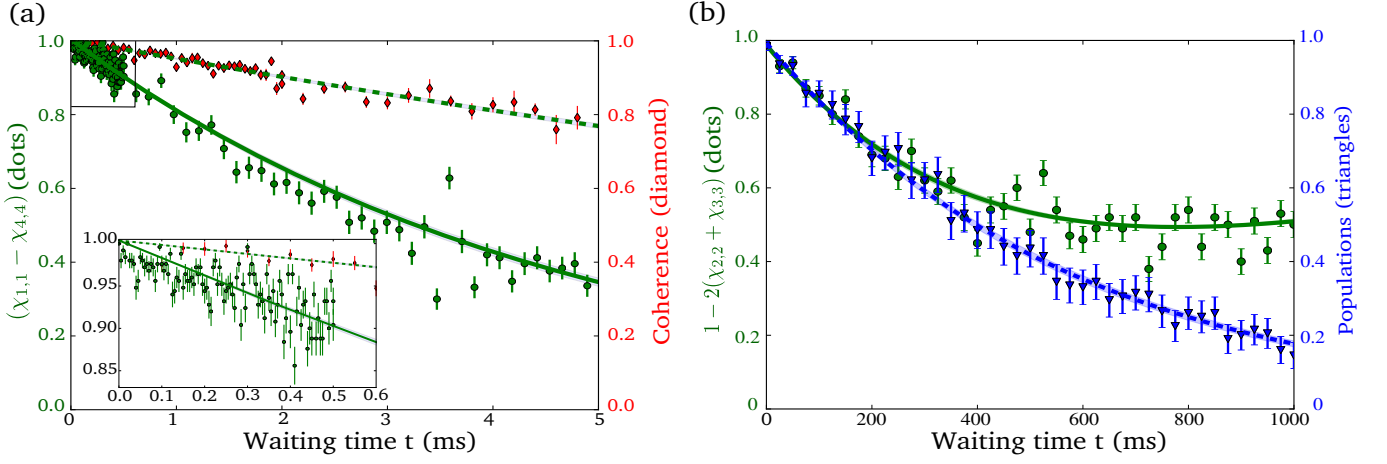


FIG. 3. (color online) Simultaneous measurement of phase decoherence (a) and the spontaneous decay (b) of a two-qubit system. The DCRT technique (green dots) is compared to a Ramsey-contrast measurement (red diamonds) and a spontaneous-decay measurement (blue triangles) (see text). The measurement using the DCRT method in (a) was carried out on the entangled two-qubit system ($\exp(-\frac{4t}{T_2^{DCRT}})$ scaling) whereas the red diamonds were measured on a single qubit with the Ramsey-contrast technique ($\exp(-\frac{t}{T_1^{rad}})$ scaling). The shaded areas correspond to the envelope of the curves with the decay times $T_{1,2}^{DCRT,rad} \pm \Delta T_{1,2}^{DCRT,rad}$, considering the statistical errors $\Delta T_{1,2}^{DCRT,rad}$. The relaxation time measurements, using the DCRT method and, in comparison, the traditional Ramsey-contrast and spontaneous decay measurement, yield: $T_2^{DCRT} = 18.8(5)$ ms, $T_2^{rad} = 19.4(8)$ ms, $T_1^{DCRT} = 1130(47)$ ms and $T_1^{rad} = 1160(30)$ ms.

- [4] J. B. Altepeter et al., Phys. Rev. Lett. **90**, 193601 (2003)
- [5] M. Mosheni, A. T. Rezakhani, and D. A. Lidar, Phys. Rev. A **77**, 032322 (2008)
- [6] M. Mosheni and D. A. Lidar, Phys. Rev. Lett. **97**, 170501 (2006)
- [7] M. Mosheni and A. T. Rezakhani, Phys. Rev. A **80**, 4 (2009)
- [8] Z. W. Wang et al., Phys. Rev. A **75**, 044304 (2007)
- [9] W. T. Liu et al., Phys. Rev. A **77**, 032328 (2008)
- [10] E. Knill et al., Phys. Rev. A **77**, 012307 (2008)
- [11] C. Schmiegelow et al., Phys. Rev. Lett. **104**, 123601 (2010)
- [12] A. Bendersky, F. Pasteski, and J. P. Paz, Phys. Rev. Lett. **100**, 190403 (2008)
- [13] A. Shabani et al., Phys. Rev. A **84**, 1 (2011)
- [14] A. Shabani et al., Phys. Rev. Lett. **106**, 1 (2011)
- [15] D. Gross et al., Phys. Rev. Lett. **105**, 250401 (2010)
- [16] M. Mosheni, A. T. Rezakhani, and A. Aspuru-Guzik, Phys. Rev. A **77**, 042320 (2008)
- [17] M. Mosheni et al., Phys. Rev. A **81**, 032102 (2010)
- [18] F. Schmidt-Kaler et al., Appl. Phys. B **77**, 789 (2003)
- [19] W. Nagourney, J. Sandberg, and H. Dehmelt, Phys. Rev. Lett. **56**, 2797 (1986)
- [20] A. Sørensen and K. Mølmer, Phys. Rev. A **82**, 1971 (2000)
- [21] G. Kirchmair et al., New J. Phys. **11**, 023002 (2009)
- [22] See appendix.
- [23] Z. Hradil, J. Rehacek, J. Fiurasek, and M. Jezek, *Quantum State Estimation* (Springer, 2004)
- [24] P. E. M. F. Mendonca et al., Phys. Rev. A **78**, 11 (2008)
- [25] B. Efron and R. Tibshirani, "Statistical science," (Institute of Mathematical Statistics, 1986) pp. 54–57
- [26] T. Monz et al., Phys. Rev. Lett. **106**, 130506 (2011)
- [27] F. Schmidt-Kaler et al., J. Phys. B: At. Mol. Opt. Phys. **36**, 623 (2003)
- [28] P. Staunum et al., Phys. Rev. A **69**, 032503 (2004)
- [29] X. Hu, R. de Sousa, and S. D. Sarma, *Foundations of Quantum Mechanics in the Light of new Technology* (eProceedings, 2001)
- [30] M. Mosheni et al., J. Chem. Phys. **129**, 174106 (2008)
- [31] J. Yuen-Zhou et al., PNAS **108**, 17615 (2011)
- [32] M. Mosheni, in preparation, 2012

Appendix

Implementation of amplitude- and phase-damping

For the complete quantum process tomography using DCQD it was considered that the process of interest only acts on the system qubit. In general due to residual light on the ancilla ion (crosstalk), it is experimentally challenging to apply single-qubit operations on one ion without affecting the second one. The unitary operations on the system ion S without affecting the ancilla ion A is experimentally implemented by the following refocusing technique: (i) Applying a global rotation $U(\frac{\pi}{2}, \phi)$ around the X or Y axis of the Bloch sphere. (ii) Shifting the phase of the second ion by π via an AC-Stark pulse $U_Z^{(2)}(\pi)$. (iii) Repetition of the first step. This effectively reduces the crosstalk, for single qubit operations roughly by a factor of 6, ideally to less than 1%.

The process of **phase damping** is implemented by the following steps (see Fig. 4(a)): (i) Hiding the population of the $D_{5/2}(m = -1/2)$ state of both ions by applying a π -pulse on the $D_{5/2}(m = -1/2) \leftrightarrow S_{1/2}(m = 1/2)$ transition. (ii) Transferring a certain amount of the population of the $S_{1/2}(m = -1/2)$ state to the $D_{5/2}(m = -5/2)$ state. The excitation probability is experimentally controlled by the pulse length t and is given by $\sin(\gamma)^2$, with $\gamma = \frac{\pi t}{T}$ and T the Rabi-oscillation period time. (iii) Repumping the transferred population into the $P_{3/2}$ state by a laser pulse at a wavelength of 854 nm whereupon the system qubit decays spontaneously into the ground state. (iv) Finally the second step is repeated to reverse the hiding process. Because of the spontaneous decay after the third step the state loses its phase information. The hiding process described in the first step is necessary to prevent the $D_{5/2}(m = -1/2)$ state from not being affected by the repumping process which would have the same effect as amplitude damping.

Amplitude damping is carried out within two steps (see Fig. 4(b)). First a certain amount of population is coherently transferred from the $D_{5/2}(m = -1/2)$ to the $S_{1/2}(m = 1/2)$ state by an addressed laser pulse analog to step (ii) of the phase damping process. Then the whole population of the $S_{1/2}(m = 1/2)$ state is transferred to the $S_{1/2}(m = -1/2)$ ground state by an optical pumping process performed by a σ^- -polarized laser beam at 397 nm exciting the ion first to the $P_{1/2}(m = -1/2)$ state followed by spontaneous decay to the $S_{1/2}(m = -1/2)$. The ancilla ion is not affected by the optical pumping process because the σ^- -polarized pulse can only excite the $S_{1/2}(m = 1/2)$ ground state.

Direct characterization of collective longitudinal and transverse relaxation processes

Let us consider a global quantum *homogenization* or *thermalization* process acting on some qubits for a time t . Thus for each single-qubit density matrix ρ , with $\rho_{00} = a$ and $\rho_{01} = b$ in the computational basis, evolves into the state $\rho(t)$ with $\rho_{00}(t) = (a - a_0)\exp(-t/T_1) + a_0$ and $\rho_{01}(t) = b\exp(-t/T_2)$, where T_1 and T_2 ($T_2 \leq 2T_1$) are relaxations and dephasing time-scales of the system, respectively. That is, the system approaches an equilibrium state identified by $a_0 \in [0, 1]$.

In order to measure these time scales using the DCQD approach we need to create quantum correlations between each pair of neighboring qubits, e.g., in the form of a Bell-state $\rho = |\Phi^+\rangle\langle\Phi^+|$ where $|\Phi^+\rangle = (|00\rangle + |11\rangle)/\sqrt{2}$, and then let all of the qubits evolve for a time t leading to state $\mathcal{E}(\rho)$. Thus by performing a Bell-state measurement between the same neighboring qubits we obtain ([16], [32]):

$$\text{Tr}[P^{11}\mathcal{E}(\rho)] - \text{Tr}[P^{44}\mathcal{E}(\rho)] = e^{-\frac{2t}{T_2}}$$

where $P^{kk'} = |B^k\rangle\langle B^{k'}|$, and $|B^k\rangle$ for $k = 1, 2, 3, 4$ corresponds to the Bell-states $|\Phi^+\rangle$, $|\Psi^+\rangle$, $|\Psi^-\rangle$, and $|\Phi^-\rangle$, respectively, where $|\Phi^\pm\rangle = (|00\rangle \pm |11\rangle)/\sqrt{2}$, $|\Psi^\pm\rangle = (|01\rangle \pm |10\rangle)/\sqrt{2}$. Using the fact that $\text{Tr}[P^{11}\mathcal{E}^T(\rho)] = \chi_{1,1}$ and $\text{Tr}[P^{44}\mathcal{E}^T(\rho)] = \chi_{4,4}$ we obtain:

$$e^{-\frac{2t}{T_2}} = \chi_{1,1} - \chi_{4,4}. \quad (5)$$

It is important to mention that this expression is only valid for Markovian noise acting on the entire system. For our system it was observed [26] that the phase decoherence of Greenberg-Horne-Zeilinger (GHZ) states scales with $\exp(-N^2t)$ instead of $\exp(-Nt)$, with N the number of ions. Therefore Eq. (1) has to be modified, which leads to the following result for the phase-decoherence:

$$e^{-\frac{N^2t}{T_2}} = \chi_{1,1} - \chi_{4,4}. \quad (6)$$

In the case of T_1 , the outcome of a BSM within the DCQD formalism yields:

$$\begin{aligned} & 1 - 2(\text{Tr}[P^{22}\mathcal{E}(\rho)] + \text{Tr}[P^{33}\mathcal{E}(\rho)]) = \\ & = (1 - 2a_0)^2(1 - 2e^{-\frac{t}{T_1}}) + (2 + 4a_0(a_0 - 1))e^{-\frac{2t}{T_1}}. \end{aligned} \quad (7)$$

For our system the equilibrium state is described by the ground state and therefore $a_0 = 1$, which leads to:

$$1 - 2(\chi_{22} + \chi_{33}) = (1 - 2e^{-\frac{t}{T_1}}) + 2e^{-\frac{2t}{T_1}}.$$

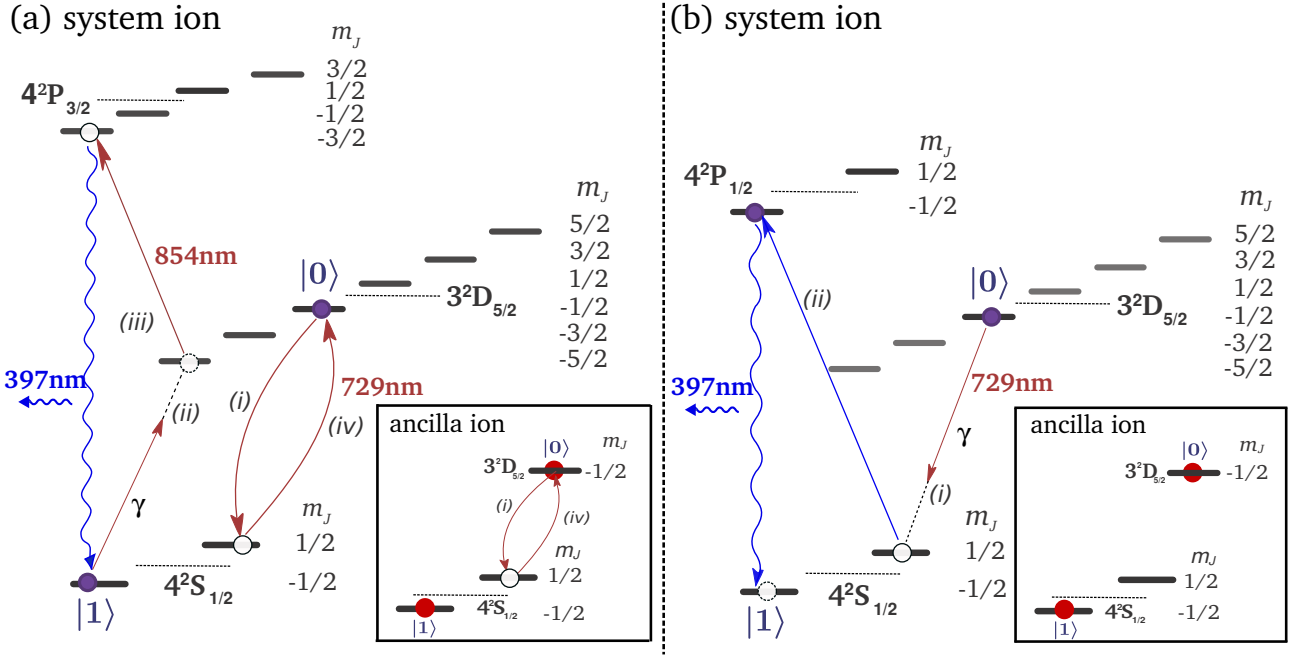


FIG. 4. (color online) Schematic of the phase damping (a) and amplitude damping (b) processes acting on the system ion S: (a) Transfer of the $S_{1/2}(m = -1/2)$ population with a probability of $\sin(\gamma)^2$ to the $P_{3/2}$ state followed by optical repumping to the ground state while the population of the $D_{5/2}(m = -1/2)$ state is hidden in the $S_{1/2}(m = 1/2)$ state. (b) The amplitude damping process is carried out by coherently transferring the population of the $D_{5/2}(m = -1/2)$ state to the $S_{1/2}(m = 1/2)$ state of the system ion followed by optical pumping to the ground state $S_{1/2}(m = -1/2)$. The ancilla ion is not affected during the whole processes, as shown in the inset figures.

For a unital quantum *homogenization* process ($\mathcal{E}(I) = I$), we have $a_0 = \frac{1}{2}$ (i.e., a completely stochastic equilibrium state). Thus the relation for T_1 becomes:

$$e^{-\frac{2t}{T_1}} = 1 - 2(\chi_{2,2} + \chi_{3,3}).$$

It is remarkable that even if we use the relations developed for the ideal DCQD scheme, assuming T_1 and T_2

acting only on the system qubit (considering the other system as a reference signal or a noiseless ancilla), we can still obtain both T_2 and T_1 only to be smaller than the actual value by a factor of 2. Note that, due to orthogonality of the BSM outcomes, it is easy to unambiguously distinguish T_1 from T_2 . Traditionally, in order to measure the longitudinal and transverse relaxation times, one needs to measure two non-commutative observables (e.g., Pauli operators σ_z and σ_x) on two sub-ensembles of identical systems.